Nucleic Acids Research, 2025, **53**, gkae1281
https://doi.org/10.1093/nar/gkae1281
Advance access publication date: 7 January 2025
Gene regulation, Chromatin and Epigenetics

Single-molecule analysis reveals that IPMK enhances the DNA-binding activity of the transcription factor SRF

Hyoungjoon Ahn[1,†], Jeongmin Yu[1,†], Kwangmin Ryu[1,†], Jaeseung Ryu[1], Sera Kim[1], Jae Yeong Park[1], Ji Kwang Kim[1], Inhong Jung[1], Haejin An[1], Sehoon Hong[1], Eunha Kim[1], Kihyun Park[1], Myunghwan Ahn[2], Sunwoo Min[1], Inkyung Jung[1], Daeyoup Lee[1], Thomas Lee[3], Youngjoo Byun[2], Ji-Joon Song[1], Jaehoon Kim[1], Won-Ki Cho[1,*], Gwangrog Lee[1,*] and Seyun Kim[1,4,5,*]

[1]Department of Biological Sciences, Korea Advanced Institute of Science and Technology (KAIST), 291 Daehak-ro, Yuseong-gu, Daejeon 34141, Republic of Korea
[2]College of Pharmacy, Korea University, 2511 Sejong-ro, Sejong 30019, Republic of Korea
[3]Department of Biochemistry, University of Colorado, 3415 Colorado Avenue, Boulder 80303, USA
[4]KAIST Institute for the BioCentury, KAIST, 291 Daehak-ro, Yuseong-gu, Daejeon 34141, Republic of Korea
[5]KAIST Stem Cell Center, KAIST, 291 Daehak-ro, Yuseong-gu, Daejeon 34141, Republic of Korea

[*]To whom correspondence should be addressed. Tel: +82 42 350 2625; Fax: +82 42 350 2610; Email: seyunkim@kaist.ac.kr
Correspondence may also be addressed to Gwangrog Lee. Email: ifglee@kaist.ac.kr
Correspondence may also be addressed to Won-Ki Cho. Email: wonkicho@kaist.ac.kr
Present addresses:
Eunha Kim, Department of Neuroscience, Korea University College of Medicine, Seoul 02841, Republic of Korea.
Sunwoo Min, Department of Biochemistry, Chungnam National University, Daejeon 34134, Republic of Korea.
[†]The first three authors should be regarded as Joint First Authors.

Abstract

Serum response factor (SRF) is a master transcription factor that regulates immediate early genes and cytoskeletal remodeling genes. Despite its importance, the mechanisms through which SRF stably associates with its cognate promoter remain unknown. Our biochemical and protein-induced fluorescence enhancement analyses showed that the binding of SRF to serum response element was significantly increased by inositol polyphosphate multikinase (IPMK), an SRF cofactor. Moreover, real-time tracking of SRF loci in live cell nuclei demonstrated that the chromatin residence time of SRF was reduced by IPMK depletion in fibroblasts. Conversely, elevated IPMK levels extended the SRF–chromatin association. We identified that IPMK binds to the intrinsically disordered region of SRF, which is required for the IPMK-induced stable interaction of SRF with DNA. IPMK-mediated conformational changes in SRF were observed by single-molecule fluorescence resonance energy transfer assays. Therefore, our findings demonstrate that IPMK is a critical factor for promoting high-affinity SRF–chromatin association and provide insights into the mechanisms of SRF-dependent transcription control via chaperone-like activity.

Graphical abstract

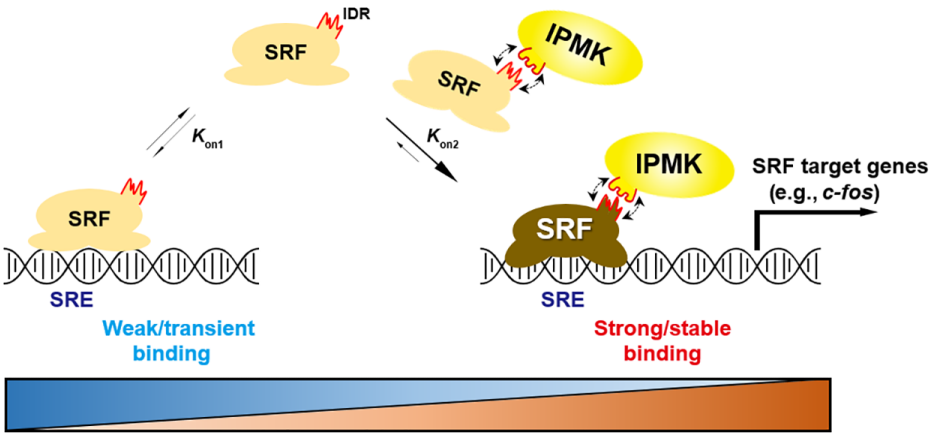

Received: September 13, 2024. **Revised:** December 9, 2024. **Editorial Decision:** December 11, 2024. **Accepted:** December 13, 2024

Introduction

Serum response factor (SRF) is a key member of the MADS (MCM1, AGAMOUS, DEFICIENS and SRF) domain-containing family of transcription factors, which is ubiquitously expressed throughout all cell types in mammals (1,2). As demonstrated by a series of *Srf* knockout (KO) and mutant mouse studies, SRF is essential for multiple biological functions in many cells including muscle cells, neurons, immune cells, hepatocytes and fibroblasts, and is therefore a key orchestrator of embryogenesis and the development of various tissues and organs (e.g. gastrointestinal tract, heart, blood vessels and immune systems) (3–8). Furthermore, several studies on experimental mouse disease models and human diseases have linked the alteration in the expression and function of SRF with disease onset and progress, suggesting that SRF plays a critical role in the pathogenesis of cancer and cardiovascular diseases (9–11).

SRF functions by binding as a homodimer to the CArG box [$CC(A/T)_6GG$] DNA sequences [also called serum response element (SRE)] within the promoters of specific genes such as *c-jun* and *c-fos* (12). This SRF–CArG association is crucial for the transcriptional activation of a diverse array of SRF target genes. SRF is known to have relatively low intrinsic transcriptional activity but its protein-protein interactions with other cofactors determine the transactivation of gene expression in a cell- and context-dependent manner (13,14). Currently, two major signaling pathways are known to act upon SRF to specify transcriptional programs (15,16). When cells are stimulated by growth factors, the mitogen-activated protein kinase signaling pathway triggers the phosphorylation of the ternary complex factor (TCF) (e.g. Elk1) coupled with SRF to drive the activation of cell growth and proliferation-related genes such as *c-fos* (15). SRF also acts as a primary transcription factor, thereby linking actin cytoskeletal dynamics with transcription (16). Through the interaction between SRF and myocardin-related transcription factor (MRTF), SRF controls the transcription of genes responsible for cytoskeleton remodeling, thus leading to cell contractility and morphological changes. Generally, the competition between TCFs and MRTFs for SRF is known to determine SRF-dependent gene expression (17,18).

Recently, inositol polyphosphate multikinase (IPMK) was identified as a key mediator of SRF action (19). IPMK is an enzyme with broad substrate specificity that catalyzes the production of inositol polyphosphates (e.g. inositol 1,3,4,5,6-pentakisphosphate) and phosphatidylinositol 3,4,5-triphosphates (20,21). Therefore, IPMK-mediated production of inositol-derived signaling second messengers modulates target proteins and related physiological functions such as cellular growth, immunity, and metabolism (22,23). In addition to its catalytic role, which is critical for inositol phosphate metabolism, IPMK non-catalytically regulates major signaling factors including mechanistic target of rapamycin (mTOR), tumor necrosis factor receptor-associated factor 6 (TRAF6), Src-associated substrate during mitosis of 68 kDa (Sam68) and the SWI/SNF complex (24–27). In yeast, IPMK (referred to Arg82) was originally identified as an essential cofactor that physically associates with the transcription factor MCM1, thereby stabilizing the transcription complex to mediate arginine-responsive gene expression (28). The discovery of the yeast transcriptional complex protein Arg82, which is able to convert inositol 1,4,5-pentakisphosphate to inositol 1,3,4,5,6-pentakisphosphate, suggested a critical role of inositol phosphates in transcriptional regulation (29). Subsequent works revealed that the lipid kinase activity of IPMK regulates the function of nuclear receptors (30). In mammalian cells, IPMK associates with SRF, a yeast ortholog of MCM1, and regulates serum-stimulated transcription of immediate early genes (IEGs; e.g. *c-fos*) (19). In IPMK KO cells and tissues, SRF was found to lose its ability to associate with its cognate SREs. Conversely, elevated IPMK levels increased DNA binding of SRF, suggesting that IPMK non-catalytically acted as a transcriptional coactivator for SRF (19). However, given that the aforementioned conclusions were mostly drawn by cell-based assays such as immunoprecipitation (IP) and chromatin IP, key fundamental questions at the molecular level remained unsolved. For example, significant challenges remain in determining whether IPMK directly or indirectly mediates SRF–DNA association, or if it impacts the structure of SRF. Furthermore, the precise role of IPMK in regulating the dynamics of SRF–chromatin interaction needs to be comprehensively defined.

Therefore, our study sought to determine the regulatory role of IPMK in SRF–DNA binding. Here, biochemical and biophysical assays, including single-molecule protein-induced fluorescence enhancement (smPIFE) (31), demonstrated that IPMK directly enhances the DNA-binding activity of SRF. Additionally, real-time tracking of chromatin-bound SRF loci in live fibroblasts demonstrated that IPMK promotes SRF chromatin residence time. Mass spectrometry analysis elucidated the key interaction interface between SRF and IPMK. Single-molecule fluorescence resonance energy transfer (smFRET) further revealed that IPMK induces structural changes in SRF. Our data indicated that IPMK is a critical cofactor for promoting SRF–DNA interaction at the molecular and cellular levels.

Materials and methods

Purification of SRF and IPMK proteins

Human SRF was cloned into a pET28a vector containing tobacco etch virus (TEV) cleavage site and expressed in *Escherichia coli* Rosetta2(DE3)pLysS at 37°C in the presence of 0.5 mM isopropyl β-D-1-thiogalactopyranoside for 2 h. Cells were harvested in 300 mM NaCl, 50 mM Tris (pH 8.0), 5% glycerol, 1% Triton-X 100, ethylenediaminetetraacetic acid-free Protease Inhibitor Cocktail (Roche) and 1 mM phenylmethylsulfonylfluoride (PMSF). The cells were sonicated on ice and centrifuged at 15 000 rpm for 15 min. Supernatants were purified by Ni-NTA agarose affinity chromatography (Qiagen) (Supplementary Figure S1). Human IPMK was expressed in Sf9 cells using a baculovirus expression vector system. Cells were harvested in 300 mM NaCl, 50 mM Tris (pH 8.0), 5% glycerol and 1 mM PMSF, then lysed by three freeze–thaw cycles in liquid nitrogen. Lysates were cleared by centrifugation at 18 000 rpm for 90 min. Supernatants were applied to Ni-NTA resins (Qiagen) with 20 mM imidazole and incubated for 2 h. The N-terminal his-tagged human IPMK was eluted with 100 mM imidazole and treated with TEV protease to remove the tag, followed by HiTrap SP HP (GE Healthcare, USA) and Superdex 200 60 600 (GE Healthcare) in a buffer containing 300 mM NaCl and 50 mM Tris-HCl (pH 8.0) (Supplementary Figure S1). Human Elk1 protein was purchased from Sino biological (12621-H20B).

Electrophoretic mobility shift assay

LightShift™ Chemiluminescent electrophoretic mobility shift assay (EMSA) Kit (Thermo Fisher Scientific, Waltham, MA, USA, #20 148) was used to conduct nonradioactive EMSA with biotinylated DNA probes. The biotin was labeled at 5′ end of oligonucleotides (Bioneer, Korea) whose sequences were sense: 5′-CTA AGC TTG CTG ACG CAG ATG TCC TAA TAT GGA CAT CCT GTC CCG GGG A-3′ and antisense: 5′-TCC CCG GGA CAG GAT GTC CAT ATT AGG ACA TCT GCG TCA GCA AGC TTA G-3′. Annealed oligonucleotides were used in the reaction. Indicated amount of proteins (SRF, IPMK, and Elk1) was incubated with oligonucleotides for 20 min at room temperature. Then, loading buffer was added to end the reaction. The reaction mixtures was electrophoresed in 7% nondenaturating polyacrylamide gel electrophoresis in 0.5× Tris-borate-ethylenediaminetetraacetic acid (TBE) buffer at 100 V for 90 min. DNA–protein complexes were transferred onto Biodyne B nylon membranes (Thermo Fisher Scientific, Waltham, MA, USA, #77 016) using 0.5× TBE for 30 min at 380 mA. The transferred complexes were cross-linked onto membranes using ultraviolet lamp equipped with 254-nm bulbs. The membrane was exposed for 15 min. The blotting was followed as described in the instruction of LightShift™ Chemiluminescent EMSA Kit.

Live-cell single-molecule tracking

For single-molecule imaging of SRF, we used custom-built microscope based on the Nikon microscope body Ti2e with highly inclined and laminated optical illumination. Images were acquired by EM-CCD camera (Andor, iXon Ultra 888), with frame rate of 10 Hz. Cells were plated on glass bottom dish (Cellvis) 1–2 days before imaging. For Halo-SRF labeling, cells were treated with media containing 10 nM of Janelia Fluor® HaloTag Ligands (JFX650 HaloTag, Promega, HT1070) for 15 min. After labeling, cells were incubated in fresh media for longer than 15 min for washing. Live cells were imaged inside the environmental chamber set at 37°C, 5% CO_2.

Residence time measurement

Residence time of SRF molecules were measured from single-molecule tracking image using ImageJ plugin TrackMate (32) and custom-built codes. Spot detection and tracking were done by TrackMate. Differences of gaussian detector was used for spot detection. Fast diffusing molecules were not detected because they were motion-blurred in long exposure time (100 ms) of each frame. Only bound molecules were detected as tracks, by strictly limiting linking distance between frames. Then, residence time of each molecule could be estimated as product of the exposure time of each frame and the length of the track. Residence time of long binding (τ_{long}) and short binding (τ_{short}) fraction were derived by biexponential fitting of cumulative distribution function of SRF residence time, using the function below (F_{long}: fraction of long binding molecule, F_{short}: fraction of short binding molecule) (33).

$$1 - \mathrm{CDF} = F_{long}\exp\left(-t/\tau_{long}\right) + F_{short}\exp\left(-t/\tau_{short}\right)$$

GST pull-down and western blotting

For GST pull-down assay, cells were washed twice with phosphate-buffered saline and lysed in lysis buffer [1% NP-40, 120 mM NaCl, 40 mM Tris-HCl (pH 7.4), 1.5 mM sodium orthovanadate, 50 mM sodium fluoride, 10 mM sodium pyrophosphate and protease inhibitor cocktail (Roche)]. Cell lysates were incubated at 4°C for 15 min, and the collected supernatants were centrifuged at 13 000 rpm for 15 min. Protein concentrations were measured by the Bradford protein assay (Bio-Rad). A total of 1.5 mg of protein lysates were applied with glutathione resin (Genescript) and incubated at 4°C for 2 h with rotation. The samples were washed three times with lysis buffer and prepared for immunoblotting. Proteins were separated by using sodium dodecyl sulphate-polyacrylamide gel electrophoresis, transferred to nitrocellulose membranes. Membranes were blocked using 5% fat-free milk for 1 h at room temperature. Primary antibodies: [GST (Cell Signaling Technology, 2622S), Flag (Sigma Aldrich, F1804), α-tubulin (Sigma Aldrich, T5168), SRF (Cell Signaling Technology, 5147), IPMK (24), c-Fos (Santa Cruz biotechnology, sc-7202), SNAP (Invitrogen, CAB4255)] diluted in 5% bovine serum albumin (BSA) were incubated overnight at 4°C with gentle rocking followed by donkey anti-mouse or goat anti-rabbit IgG conjugated to horseradish peroxidase (HRP) for 1 h at room temperature. The HRP signals were developed with the Clarity ECL substrate (Bio-Rad) and SuperSignalTM West Femto Maximum Sensitivity Substrate (Thermo Fisher Scientific), and measured by using a Chemi-Doc imaging system (Bio-Rad).

Generation of Halo-tagged SRF cell line

Ipmk-floxed mouse embryonic fibroblasts ($Ipmk^{fl/fl}$ MEFs) were cultured at 37°C in 5% CO_2 in DMEM (Welgene) supplemented with 10% fetal bovine serum (FBS) (Gibco) and 100 U/ml penicillin and 100 μg/ml streptomycin (HyClone) (24). For live cell tracking of endogenous SRF, HaloTag was N-terminally fused to SRF with CRISPR knock-in. Single-guide RNA (sgRNA) sequence targeting SRF gene was cloned into pX459 (Addgene #62 988). Plasmid containing homology arm for CRISPR knock-in was synthesized (Bionics). HaloTag sequence was cloned in between the homology arms to generate Halo-SRF repair template vector. SRF-targeting pX459 and Halo-SRF repair template were cotransfected into $Ipmk^{fl/fl}$ MEF, using FuGene HD (Promega). Transfected cells were cultured for 3 days and labeled with JF549-HaloTag Ligand (Promega). Then positive cells expressing Halo-SRF were sorted with FACS (Bio-rad). All sequences used in the CRISPR knock-in procedure are available in the Supplementary Table S1. Lentiviruses (Lenti-GFP and Lenti-GFP-Cre) were generated in HEK293T cells by transfecting the lentiviral plasmids with packing vector (PAX2.0) (Addgene #12 260) and envelop plasmids (MD2.G) (Addgene #12 259). Lentiviruses were added to Halo-SRF $Ipmk^{fl/fl}$ MEFs after 8 h and the stable gene expression was selected in medium supplemented with puromycin for 48 h. Then, the green fluorescent protein (GFP)-positive cells were sorted by FACS (Moflo Astrios EQ, Beckman Coulter).

Transfection and FACS

For IPMK overexpression, Halo-SRF $Ipmk^{f/fl}$ MEFs were transfected with SNAP or SNAP-human IPMK expression vector using FuGene HD (Promega). Next day, transfected cells were subcultured to glass bottom dish for imaging, or FACS sorted for western blotting. Transfected cells were labeled with media containing 100 μM SNAP-Cell® TMR-Star

(New England Biolabs) for 30 min, and washed in fresh media. For imaging, TMR-labeled cells were manually selected on the microscope for single molecule tracking. For western blotting analysis, TMR-positive cells were sorted with FACS (Bio-Rad S3e).

Chromatin immunoprecipitation

For chromatin immunoprecipitation (ChIP) assay, magnetic beads were washed with radioimmunoprecipitation assay (RIPA) wash buffer and incubated with either normal rabbit IgG (Cell Signaling Technology, 2729) or anti-SRF (Cell Signaling Technology, 5147) antibodies. MEFs were resuspended with Dulbecco's phosphate-buffered saline (DPBS) containing 1% FBS and fixed by adding 2 mM disuccinimidyl glutarate (DSG) and 10% formaldehyde to cross-link protein and DNA. After fixation, cells were sonicated with 1% sodium dodecyl sulfate (SDS) lysis buffer and immunoprecipitated with antibody-conjugated magnetic beads for 4 h. The incubated magnetic beads were washed with RIPA wash buffer and incubated with 1× Tris buffer containing 10% SDS, RNAse A and proteinase K at 65°C, overnight. After incubation, the supernatants of cell lysates were transferred to Ampure XP beads and incubated for 5 min at room temperature. After eliminating the supernatants, the beads were washed with 80% ethyl alcohol and the chromatin fragments were eluted with 1× Tris buffer. ChIP primers were as follows: mouse *c-fos* promoter SRE-153, 5′-CGTCAATCCCTCCCTCCTTT-3′, mouse c-*fos* promoter SRE-338, 5′-CCGTCTTGGCATACATCTTT-3′.

Generation of SRF KO cell line with CRISPR/Cas9

For SRF KO, sgRNAs were designed to target exon 1 of mouse SRF gene using an online platform (34). The guide RNA (gRNA) sequence used was 5′-AGCTCGGCGTGGTGGTCGGT-3′. The target oligo was cloned into the lentiCRISPRv2 vector as previously described (35). These cloned lentiCRISPRv2 vectors were transfected into HEK293T cells along with PAX2 and MD2.G vectors using the jetPRIME transfection reagent (Polyplus Transfection) according to the manufacturer's instructions. Transfected HEK293T cells were cultured in DMEM supplemented with 10% FBS and 1 mM sodium pyruvate for 48 h. The produced lentiviruses were filtered using a 0.45 μm syringe filter. For viral transduction, NIH3T3 cells were incubated in the filtered viral media overnight. Transduced NIH3T3 cells were then selected using puromycin and confirmed by western blotting.

Hydrogen–deuterium exchange mass spectrometry

a. Sequencing (liquid chromatography-tandem mass spectrometry (LC-MS/MS))

To identify peptic fragments of SRF and IPMK, 100 pmoles of each protein (5 μl) were mixed with 45 μl of the sample buffer [50 mM Tris (pH 7.4), 100 mM sodium chloride] and then mixed with 50 μl of a quenching buffer (3 M guanidine HCl, 1.5% formic acid). The whole sample (100 μl total) was injected into a Waters hydrogen/deuterium exchange with liquid chromatography (HDX-LC) box (Waters) in which protein was digested by an online pepsin column (Waters Enzymate BEH pepsin column, 2.1 × 30 mm, 5 μm). The resulting peptic peptides were trapped and desalted on a Waters ACQUITY UPLC BEH C4 1.7 μm VanGuard Pre-column (2.1 × 5 mm) at 100 μl/min Buffer A (0.1% formic acid in water) for 3 min. The digestion chamber was kept at 15°C and the trap and analytical columns were at 0°C. The peptides were eluted with 3–33% Buffer B (0.1% formic acid in acetonitrile) between 0 and 6 min, 33–40% B between 6 and 6.5 min and 40–85% B between 6.5 and 7 min. The eluted peptides were resolved on a Waters ACQUITY UPLC Protein BEH C4 column (300 Å, 1.7 μm, 1 × 50 mm). MS/MS spectra were performed on a Thermo LTQ orbitrap Velos mass spectrometer. The peptides were ionized using electrospray ionization with the source voltage = 5.0 kV and S-lens radio frequency (RF) level = 60%. The capillary temperature was 275°C and the source heater was off. The sheath gas flow was 10. Precursor ions were scanned between 350 and 1800 m/z at 60 000 resolution with automatic gain control (AGC) 1×10^6 (max ion fill time = 500 ms). From the precursor scan, the top 10 most intense ions were selected for MS/MS with 180 s dynamic exclusion (10 ppm exclusion window, repeat count = 1) and AGC 1×10^4 (max ion fill time = 100 ms) Ions with unassigned charge states were rejected for MS/MS. The normalized collision energy was 35%, with activation Q = 0.25 for 10 ms.

MS/MS spectra were searched against a database consisting of SRF and IPMK protein sequence in a FASTA format using the MaxQuant/Andromeda program (version 1.6.3.4) developed by the Cox Lab at the Max Planck Institute of Biochemistry (36,37). The digestion mode was 'unspecific' and oxidation of methionine was set as a variable modification. The minimum peptide length for the unspecific search was 8. MaxQuant/Andromeda used 4.5 ppm for the main search peptide tolerance and 0.5 Da for MS/MS tolerance. The false discovery rate was 0.01. A list of peptides identified from the search was used as an exclusion list for the next round of LC-MS/MS and a total of three LC-MS/MS were performed for each protein.

b. Hydrogen–deuterium exchange

Ten 250 μl aliquots of the sample buffer were dried using vacuum centrifugation, and reconstituted with an equal volume of deuterium oxide ('D_2O buffer'), and put in a 20°C water bath. SRF (37.5 μl) was mixed with either IPMK (37.5 μl) or the sample buffer (37.5 μl) and pre-incubated on ice for at least 30 min to ensure the complex formation. Ten minutes prior to the initiation of the hydrogen–deuterium exchange (HDX) reaction, 10 μl of the preincubated sample was transferred to a 0.5 ml tube and incubated at 20°C. The HDX reaction was initiated by the addition of the D_2O buffer (40 μl) to the 10 μl sample (80% D_2O final). The reaction was quenched at 0.5, 1, 2 and 4 min after the initiation by adding the quench buffer (50 μl). The whole sample (100 μl) was injected into the Waters HDX-LC box and LC-MS was performed as described in the above section. For the HDX samples, only MS1 spectra were recorded and each time point was measured in triplicates.

c. Data analysis

The hydrogen–deuterium exchange mass spectrometry (HDX-MS) data were analyzed using Mass Spec Studio (version 2.4.0.3484) developed by the Schriemer lab at the University of Calgary (38,39). 'Peptide.txt' and 'evidence.txt' from

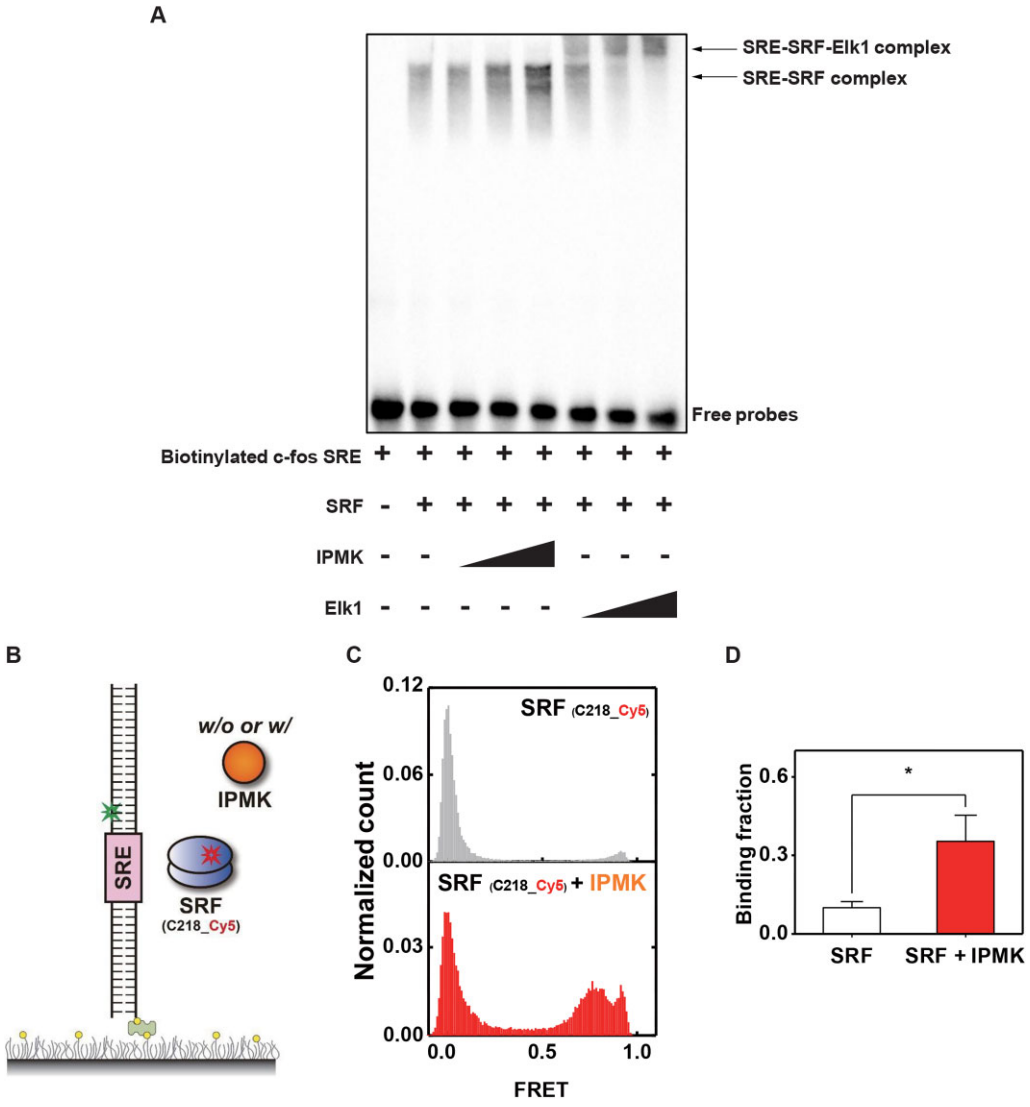

Figure 1. Single-molecule characterization of SRF binding to SRE in the absence or presence of IPMK. (**A**) EMSA using 1 nM of 5′ biotinylated *c-fos* DNA probe (SRE) and recombinant His-SRF (25 nM), GST-His-Elk1 (25, 50, 100 nM) and IPMK (25, 50, 100 nM). (**B**) Schematic of single-molecule binding assay of Cy5-SRF to Cy3-SRE. (**C**) smFRET histogram of binding of SRF at 15 nM to SRE after 10-min incubation in the absence (top) or presence (bottom) of IPMK at 100 nM. (**D**) Binding fraction of (**C**) with mean ± standard error of the mean (SEM) (n = 3). One-tailed unpaired *t*-test, $P = 0.03$.

the MaxQuant/Andromeda search results were used to generate the 'identification' table for Mass Spec Studio using an in-house Python script. The raw files from the Thermo LTQ orbitrap Velos were converted to mzML files using ProteoWizard (version 3.0.20216, 64 bit). The default processing parameters were used except mass tolerance = 15 ppm, total retention time width = 0.15 min, XIC smoothing = Savitzky Golay Smoothing and deconvolution method = centroid. All processed data were manually validated and for peptides showing bimodality in isotopic distribution, the 'is EX1' option was on to estimate both 'fast' and 'slow' HDX modes.

smPIFE and FRET

All DNA oligos were purchased from Integrated DNA Technologies, and amine-modified oligos were labeled with NHS-Cy3 (Cytiva) or NHS-Alexa488 (Thermo Fisher Scientific). DNA sequences and modifications are listed in Supplementary Table S2. For double-stranded (ds) SREs used in Figure 1, 2, 5 and 6, SRE1 (Cy3) and SRE1 (Alexa488) oligos (Supplementary Table S2) were annealed with Biotin-SRE2 oligo in a buffer containing 10 mM Tris-HCl (pH 8.0) and 50 mM NaCl at 90°C for 3 min, and then slowly cooled to room temperature. The ds SREs were immobilized via the biotin-neutravidin interaction on a flow chamber that assembled with a PEGylated quartz slide and a cover slip (40). For ds SREs used in Figure 7, SRE1 and SRE2 (Supplementary Table S2) were annealed as above.

The only exposed cysteine 218 (C218) on SRF and $SRF^{\Delta 220–236}$ was successfully labeled with maleimide-Cy5 (Cytiva) for SRF (C218_Cy5) and $SRF^{\Delta 220–236}$ (C218_Cy5) (41). For double-labeling of SRF and $SRF^{\Delta 220–236}$ with Cy3 and Cy5, SRF and $SRF^{\Delta 220–236}$ were labeled with CoA-Cy3 at the N-terminal ybbR-tag and with maleimide-Cy5 at the C218 (42). After labeling, the labeled SRF and $SRF^{\Delta 220–236}$ were purified with Ni-NTA resin (QIAGEM) to remove excess free dye. The sample was dialyzed with a storage buffer [50 mM Tris-HCl (pH 8.0), 300 mM NaCl and 5% glycerol] and was divided into small aliquots. The aliquots were frozen in liquid nitrogen and stored at −80°C.

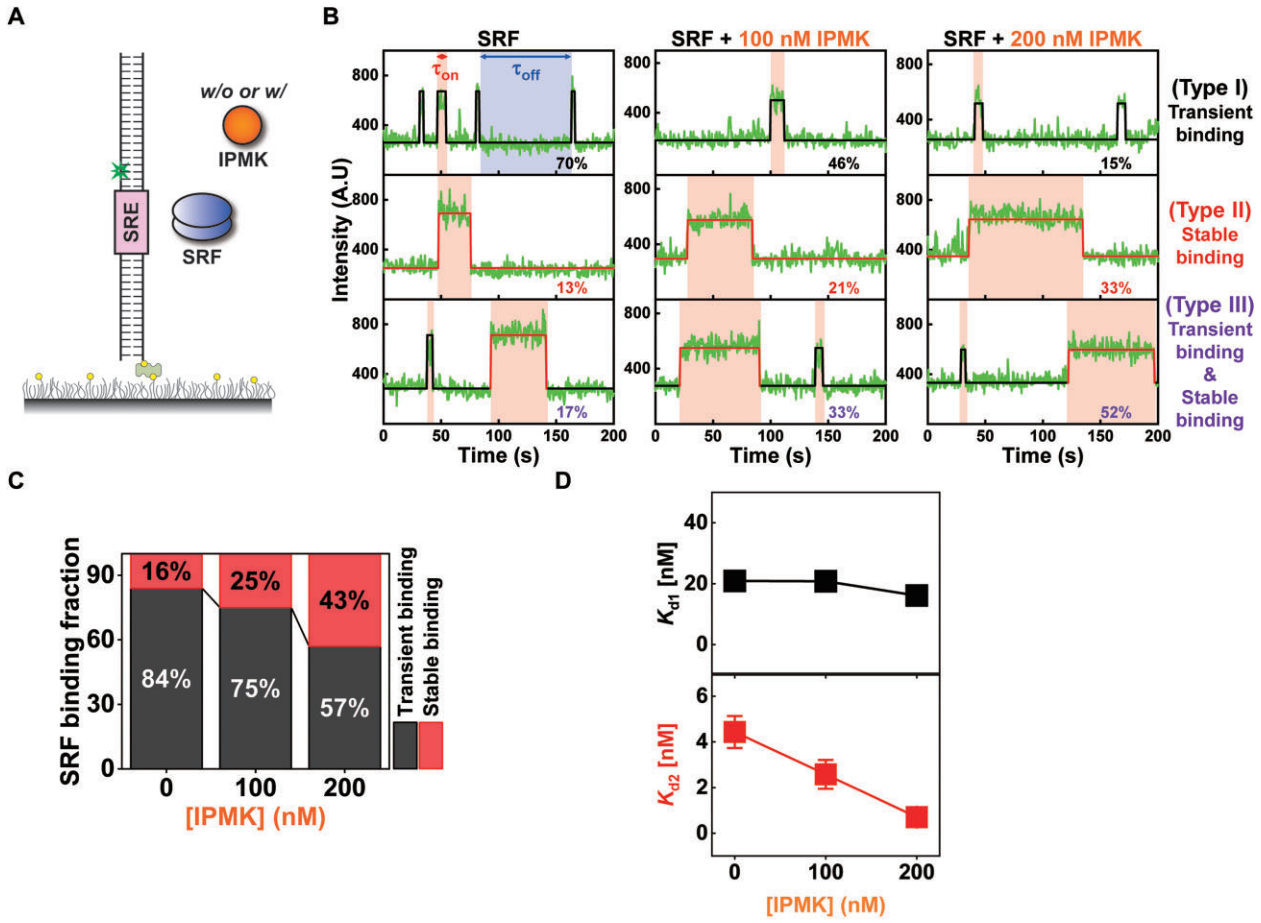

Figure 2. Quantitative analysis of SRF-SRE binding kinetics facilitated by IPMK via smPIFE. (**A**) Schematic of smPIFE assay on Cy3-SRE. (**B**) Representative intensity-time trajectories. When SRF binds to DNA in the vicinity of SRE, the intensity of Cy3 increases due to the photochemical property of Cy3-SRE. The IPMK concentration was increased from 0 nM (left) to 100 nM (middle) to 200 nM (right) in the presence of SRF at 5 nM. Bound (τ_{on}) and unbound (τ_{off}) times are shown in pink and sky blue regions, respectively. All trajectories were classified into three categories: transient binding (type I, top), stable binding (type II, middle) and a combination of transient and stable binding (type III, bottom). The percentage of each trajectory type was analyzed and shown in the bottom-right corner of each panel. (**C**) SRF binding fraction was plotted as function of IPMK concentration. Bound times $\leq$ 35 s were assigned to transient binding events (red) whereas bound times $>$ 35 s to stable binding events (dark gray) based on the analysis in Supplementary Figure S3. The cutoff time at ~35 s, which discriminates between transient and stable binding, was chosen as the time to start to saturate the stable binding (Supplementary Figure S3D). This time point was reasonable for the time range shown in Supplementary Figure S3A and C. (**D**) IPMK-concentration-dependence of K_{d1} and $K_{d2,}$ obtained from double exponential decays of bound times (see Supplementary Figure S3). The values of K_{d1} were determined as $\tau_{off} \times$ [SRF]) / τ_{on1}, and those of K_{d2} were determined as $\tau_{off} \times$ [SRF]) / τ_{on2}, where τ_{on1}, τ_{on2}, and τ_{off} were the values obtained in Supplementary Figure S3.

For smPIFE and smFRET assay, SRFs and SRF$^{\Delta 220-236}$s were injected with or without IPMK in the imaging buffer containing 10 mM Tris-HCl (pH 7.5), 50 mM KCl, 10 mM dithiothreitol (DTT), 100 μg/ml BSA, 1 mg/ml Trolox (Sigma–Aldrich), 1 mg/ml glucose oxidase (Sigma–Aldrich), 0.03 mg/ml catalase (Sigma–Aldrich) and 1% (*v*/*v*) dextrose (Sigma–Aldrich). For protein immobilization experiments as illustrated in Figure 7, doubly labeled SRF or SRF$^{\Delta 220-236}$, each containing a 6xHis tag at N terminus, was co-incubated with a 5-fold molar excess of their corresponding unlabeled variants. The proteins were immobilized by the nickel-histidine interaction onto a PEGylated quartz slide, which had been sequentially coated with biotinylated NTA and $NiSO_4$. The chamber was rinsed with the imaging buffer to eliminate any unbound proteins. To assess protein interactions, 100 nM of SRE and/or 100 nM of IPMK were subsequently introduced into the imaging buffer.

The flow chamber was illuminated with 488 nm or 532 nm laser (Coherent). The fluorescence intensities were collected using home-built prism-type total internal reflection fluorescence microscope (IX71, Olympus) and EMCCD (iXon Ultra 897, Andor) with 100 or 500 ms resolution (40). The FRET efficiency (E_{FRET}) was calculated by the equation $E_{FRET} = (I_A - \alpha \times I_D) / (I_A + I_D)$, where α is the leakage correction factor, I_D and I_A are the intensities of the donor (Cy3) and acceptor (Cy5). All the data were analyzed with MATLAB (Mathwork) and Origin (OriginLab).

The suitability of the fit for estimating the τ_{on} and τ_{off} values in the histograms was assessed using Akaike information criterion (AIC) and Bayesian information criterion (BIC) by the equations $AIC = 2k - 2\ln(L)$ and $BIC = k\ln(n) - 2\ln(L)$, where L is the likelihood, k is the number of parameters and n is the number of data points (43,44).

In silico modeling method

Crystal structure of DNA-binding SRF in PDB format was downloaded from RCSB protein data bank (PDB ID: 1SRS). For extended amino acid residues 220–236 of SRF, a homology model of human SRF in Alphafold (UniProt: P11831) was developed and downloaded from Alphafold structure database (https://alphafold.ebi.ac.uk) as PDB and FASTA format. Two models were then superimposed with Discovery studio 3.1 Visualizer. The active site regions were represented as ball and stick mode with current selection (red sphere) at around 7.5 Å radius (220–230) or loop structure (231–236).

Results

IPMK enhances the DNA-binding activity of SRF *in vitro*

Previous studies using ChIP assays demonstrated that the interactions between SRF and SRE were markedly reduced in IPMK-depleted fibroblasts and brain tissues (19). Introduction of a dominant negative peptide that interferes with IPMK-SRF binding further diminished SRF-SRE interactions (19). This leads us to propose that IPMK may play a crucial role in promoting protein–DNA interaction between SRF and SRE. This possibility was first examined via EMSA to determine the direct effect of IPMK on the binding of SRF to SRE. IPMK alone did not form a complex with the SRE in EMSA (Supplementary Figure S2A), suggesting that IPMK has no DNA-binding activity. Interestingly, we observed that IPMK significantly enhanced the DNA binding activity of SRF in a dose-dependent manner (Figure 1A and Supplementary Figure S2A and B). The specificity of the SRF–SRE interaction was verified with mutant SRE oligonucleotide, which did not form complexes (Supplementary Figure S2C). The catalytically inactive, mutant K129A IPMK (19,24) also promoted SRF–SRE binding (Supplementary Figure S2D), indicating that IPMK's effect on the SRF–DNA interaction occurs independently of its kinase activity. In the presence of IPMK, there were no changes in the migration of the SRF–DNA complex, whereas an SRF cofactor, Elk1, resulted in a high molecular weight supershift signal, which indicated the presence of an SRF–Elk1–DNA complex (Figure 1A). This result is likely due to a weak interaction between IPMK and SRF, meaning that IPMK dissociates from SRF–DNA complexes during electrophoresis conditions, which is similar to other TF complexes (e.g. AP-1–NF-κB, HMG–HOXD9) (45,46). Since ternary protein–DNA complexes were not detectable under conventional EMSA conditions, the enhancement of DNA-binding activities of NF-κB and HOXD9 by their cofactors, AP-1 and HMG1, was validated by demonstrating interactions between AP-1–NF-κB and HMG1–HOXD9 using other techniques such as bimolecular fluorescence complementation-based FRET assay or chromatography analysis (45,46).

To further scrutinize the interaction at the single-molecule level between the SRF and SRE in the absence or presence of IPMK, the DNA substrate containing SRE was tethered to a polymer-coated surface via the biotinylated end (Figure 1B). For the detection of smFRET, SRF was site-specifically labeled at C218 with the acceptor, Cy5 (termed Cy5-SRF), and the DNA substrate (Figure 1B) was labeled with the donor (Cy3) ∼3 base pairs away from the SRE (termed Cy3-SRE). In the experimental configuration, FRET values higher than ∼0.6 were expected when the Cy5-SRF protein was bound to the Cy3-SRE substrate. In the absence of IPMK, minimal binding activity was observed in the FRET region, with FRET values higher than ∼0.6 (top panel in Figure 1C). In contrast, significantly enhanced binding of Cy5-SRF to the Cy3-SRE was observed in the high FRET region when IPMK was present (bottom panel in Figure 1C and D), consistent with EMSA (Supplementary Figure S2E), validating that our labeling strategy. These consistent results suggest that modifications and labeling of DNA and proteins have minimal effects. Taken together, our findings suggest that IPMK certainly facilitates the interaction between SRF and SRE, explaining the EMSA data (Figure 1A).

We next monitored real-time binding events at the single-molecule level using protein-induced fluorescence enhancement (PIFE), which occur when SRF binds and dissociates into the Cy3-SRE substrate in the presence or absence of IPMK (Figure 2A). PIFE has two major advantages: (1) when a non-labeled protein binds to a DNA region close to Cy3, the intensity of Cy3 increases so that the binding of the non-labeled protein to the DNA can be easily observed by labeling only DNA with Cy3; (2) the imaging background does not increase when the concentration of unlabeled protein increase, thus enabling the real-time monitoring of DNA binding events as a function of protein concentration (31).

The individual binding events of SRF to SRE (Figure 2B) were analyzed by increasing the IPMK concentration from 0 nM (Figure 2B, left) to 100 nM (Figure 2B, middle) and finally to 200 nM (Figure 2B, right). Binding time trajectories revealed transient and stable binding events regardless of IPMK concentration (Figure 2B). More specifically, binding time trajectories can be divided to three types: transient binding (type I, top), stable binding (type II, middle), and the coexistence of both events (type III, bottom) (Figure 2B). As the concentration of IPMK increased, the proportion of type I decreased (e.g. 70%→46%→15%) (Figure 2B, top), while the proportions of types II and III increased (e.g. 13%→21%→33% and 17%→33%→52%, respectively) (Figure 2B, middle and bottom). Overall, the population of transient binding events decreases with increasing IPMK concentration (e.g. 84%→75%→57%) and that of stable binding events increases with increasing the IPMK concentration (e.g. 16%→25%→43%) (Figure 2C). The bound times (τ_{on}, pink region) and unbound times (τ_{off}, sky blue region) of individual trajectories were measured as a function of IPMK concentration. The distribution of bound times was fitted to a double exponential decay with two characteristic decaying times (τ_{on1} and τ_{on2}), whereas that of unbound times was fitted to a single exponential decay with a single decay time (τ_{off}) (Supplementary Figure S3A–G). The fitting was validated using the AIC (43) and the BIC (44), as detailed in the 'Materials and methods' section (Supplementary Table S3). This indicates there are two rate constants associated with binding events: one transient (black in Supplementary Figure S3A and C) and the other stable (red in Supplementary Figure S3A and C). Further analyses revealed that the equilibrium constant (black in Figure 2D) obtained from the transient and short binding events exhibited an IPMK-concentration-independent property, whereas that from the stable and long binding events displayed an IPMK-concentration-dependent behavior (red in Figure 2D). Moreover, analysis of FRET

traces using the Cy5-SRF further corroborates our findings, as indicated by consistent results (Supplementary Figure S4).

These results suggest that the stable SRF-SRE complexes, which were bound to DNA for longer times, were affected and generated by the interaction with IPMK. To further verify whether the effect of IPMK was due to a crowding effect, BSA was added at the same concentration as IPMK as a control instead of IPMK. As expected, there was no difference between SRF alone (left in Supplementary Figure S3A and E) and SRF with BSA (Supplementary Figure S3C and G) for τ_{on1}, τ_{on2}, and τ_{off}. Unlike SRF, IPMK did not specifically bind to DNA, as it is not a transcription factor of SRE, and few events with very short binding times were considered non-specific binding. These findings suggest that the enhanced binding activity of SRF to SRE was indeed due to the interaction with IPMK.

SRF residence time is controlled by IPMK at the cellular level

We next investigated the functional role of IPMK in regulating the binding affinity of SRF binding affinity to its DNA target sites at the cellular level. We firstly performed a loss-of-function experiment by eliminating IPMK in cells. To achieve IPMK KO, we utilized *Ipmk*-floxed MEFs (*Ipmk*$^{fl/fl}$ MEFs). To enable real-time tracking of endogenous SRF in live *Ipmk*$^{fl/fl}$ MEF cells, we tagged endogenous SRF with HaloTag (Halo-SRF) through the CRISPR knock-in approach (Figure 3A). To determine whether IPMK contributes to SRF–DNA binding in cells, as previously observed *in vitro* with PIFE, we measured residence time of DNA-bound SRF molecules with time lapse imaging of sparsely labeled Halo-SRF in GFP-expressing wild-type or IPMK KO MEFs (Figure 3B and C and Supplementary Movie 1).

To detect only bound molecules of labeled SRFs within live cell nuclei, we performed time-lapse imaging with an exposure time of 100 ms. Under this condition, rapidly diffusing SRFs are blurred into the background, rendering them undetectable. Based on our *in vitro* single-molecule assay results, we set the interval of time-lapse imaging to 5-s to minimize photobleaching effects while capturing both transient and stable binding events (Figure 3C, left). The imaging results enabled us to track SRF molecules that were strictly bound to specific loci within live cell nuclei. The movement of bound SRFs observed in representative kymographs reflects the motion of the live cell within the fixed region of interest during tracking (Figure 3C, right).

Consistent with previous studies, the residence time of SRF was shown in two populations, short-binding and long-binding, and was well-fitted with a double-exponential decay model representing both short- and long-bound transcription factor molecules in the nuclei of live cells (33,47). The long-binding population is considered to represent stable-binding of SRF to DNA target sites, while short-binding population is thought to indicate transient-binding to DNA. Our results showed that wild-type MEFs, expressing endogenous levels of SRF and IPMK, exhibited a long-binding time of 115.7 s for SRF, which aligns with previous studies and our PIFE data. Notably, we found that the residence time of long-bound SRF significantly decreased to 99.9 s in IPMK KO cells (Figure 3D and E), indicating that endogenous IPMK enhances SRF–DNA binding *in vivo*. In contrast, consistent with our PIPE assay results, the residence time of short-bound SRF remained unaffected by the presence or absence of IPMK (Supplementary Figure S5A). Meanwhile, the fraction of long-bound and short-bound SRF remained unchanged in IPMK KO cells (Supplementary Figure S5B).

To find out whether the altered binding of SRF following IPMK depletion is indeed relevant to its specific target DNA sequence, we performed ChIP-quantitative PCR (qPCR) with SRF for the SRE of the *c-fos* gene (*c-fos* SRE). In wild-type MEFs, we observed significant enrichment of *c-fos* SRE in SRF-bound DNA. However, this enrichment was markedly reduced to near the basal level in IPMK KO MEFs (Supplementary Figure S6A). Furthermore, the induction of c-Fos protein upon serum stimulation was abolished in IPMK KO cells (Supplementary Figure S6B). These findings indicate that IPMK is essential for the stable binding of SRF to its specific binding sites and for the proper activation of target genes.

Furthermore, given that the effect of IPMK on SRF–DNA binding is stoichiometric *in vitro*, we measured the residence time of SRF upon IPMK overexpression in MEFs, which corresponds to a gain-of-function experiment (Figure 3F and G, and Supplementary Figure S5C). Remarkably, an increased amount of IPMK led to a substantial increase in the SRF long-binding time, from 116.9 to 142.4 s (Figure 3H and I). Unlike the IPMK KO condition, an increase in the residence time of short-bound SRF was observed with IPMK overexpression (Supplementary Figure S5D). This effect is likely attributed to a statistical artifact in the analysis of the total population, influenced by an increase in the residence time of long-bound SRF. We note that, the fraction of long- and short-bound SRF remained unchanged with IPMK overexpression, as observed in the IPMK KO condition (Supplementary Figure S5E). These findings suggest that SRF–DNA binding is sensitive to changes in IPMK concentration around its endogenous level, revealing an additional layer of regulation for SRF activity within the cells.

SRF intrinsically disordered regions 220–236 interacts with IPMK

To gain insights into the underlying molecular basis for the IPMK action on SRF, we measured HDX on SRF in the presence *vs* absence of IPMK using mass spectrometry. A total of 85 peptides encompassing 85.05% of the primary sequence of SRF were analyzed (Supplementary Figure S7A and B). Of those, a single peptide (res. 220–236) showed a significant decrease in exchange at the shortest time point (0.5 min, $P < 0.01$) (Figure 4A), suggestive of a potential IPMK-binding site. Given that the intrinsically disordered regions (IDR) of IPMK mediate SRF binding (19,48), we next sought to assess whether IPMK-SRF interaction occurs via IDR–IDR interaction. To achieve this, we searched for disordered regions of the amino acid sequence of SRF using PONDR-VL (49), a previously validated algorithm, and found that the SRF 220–236 peptide exhibited a highly significant disorder score (Figure 4B). Mapping of these protected regions on the crystal structure of SRF (50) revealed that the IPMK-binding SRF 220–236 IDR site spans across the transactivation domain next to the dimerization interface (Figure 4C).

To confirm the involvement of this peptide in IPMK-SRF binding, we next deleted amino acids 220–236 of SRF (SRF$^{\Delta 220–236}$) and performed co-immunoprecipitation in HEK293T cells. The interactions between IPMK and the SRF$^{\Delta 220–236}$ mutant were markedly reduced compared to the wild-type SRF (SRF^{WT}) (Figure 4D), demonstrating the spe-

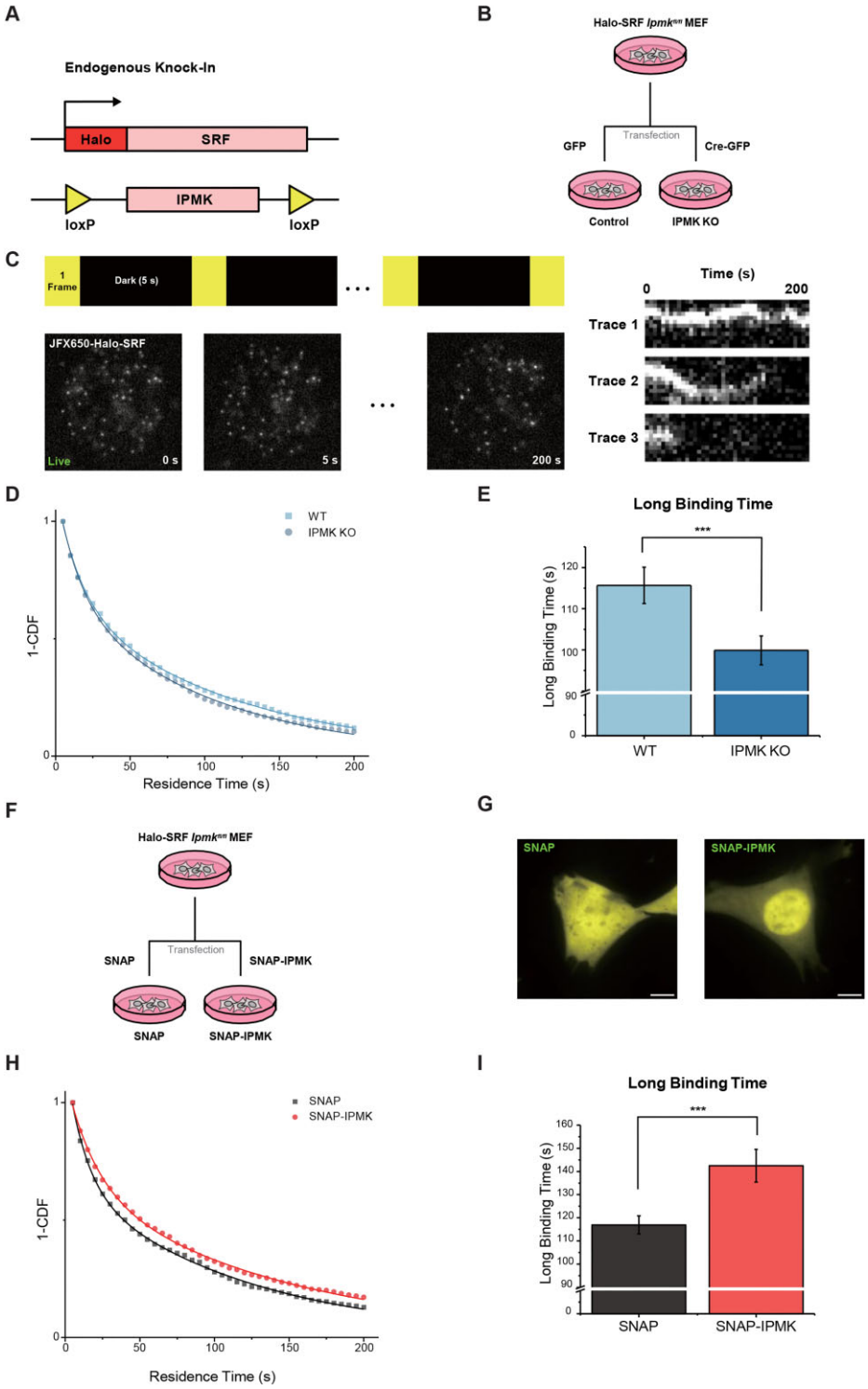

Figure 3. Measurement of SRF residence time upon IPMK depletion or overexpression in live cells. (**A**) HaloTag is inserted at the N-terminus of endogenous SRF gene in *Ipmk*$^{fl/fl}$ MEFs by CRISPR/Cas9 targeted genome editing, for single molecule tracking of SRF. (**B**) IPMK KO cells were generated by transduction of *Ipmk*$^{fl/fl}$ MEFs with adenovirus carrying the gene encoding the Cre recombinase. (**C**) Left: Schematic and representative image of single-molecule tracking. Halo-SRF was sparsely labeled with JFX650. Right: Representative kymographs of tracked SRF molecules with different residence times. (**D**) Complement cumulative distribution functions (dots) and their biexponential fittings (lines) of SRF residence times in control and IPMK KO (three replicates combined, total n_{cells} = 23,23 for each group). (**E**) Estimated residence times of long-binding population of SRF molecules in (**C**). (**F**) Overexpression of IPMK in Halo-SRF *Ipmk*$^{fl/fl}$ MEFs by transfection. (**G**) Representative images of SNAP or SNAP-IPMK transfected cells labeled with SNAP TMR-STAR. (**H**) Complement cumulative distribution functions (dots) and their biexponential fittings (lines) of SRF residence times in control and IPMK overexpressing cell (three replicates combined, total n_{cells} = 17,17 for each group). (**I**) Estimated residence times of long-binding population of SRF molecules in (**H**). Bi-exponential fitting was used for the estimations. (Error bars represent 95% confidence interval. Difference was significant with ***: 99.9% confidence interval.) A total of 1107, 1373, 799 and 909 single-molecule traces were acquired for quantification of residence times and binding fractions in live cells of *Ipmk*$^{fl/fl}$ WT control, *Ipmk*$^{fl/fl}$ KO, SNAP-only overexpression and SNAP-IPMK overexpression conditions, respectively.

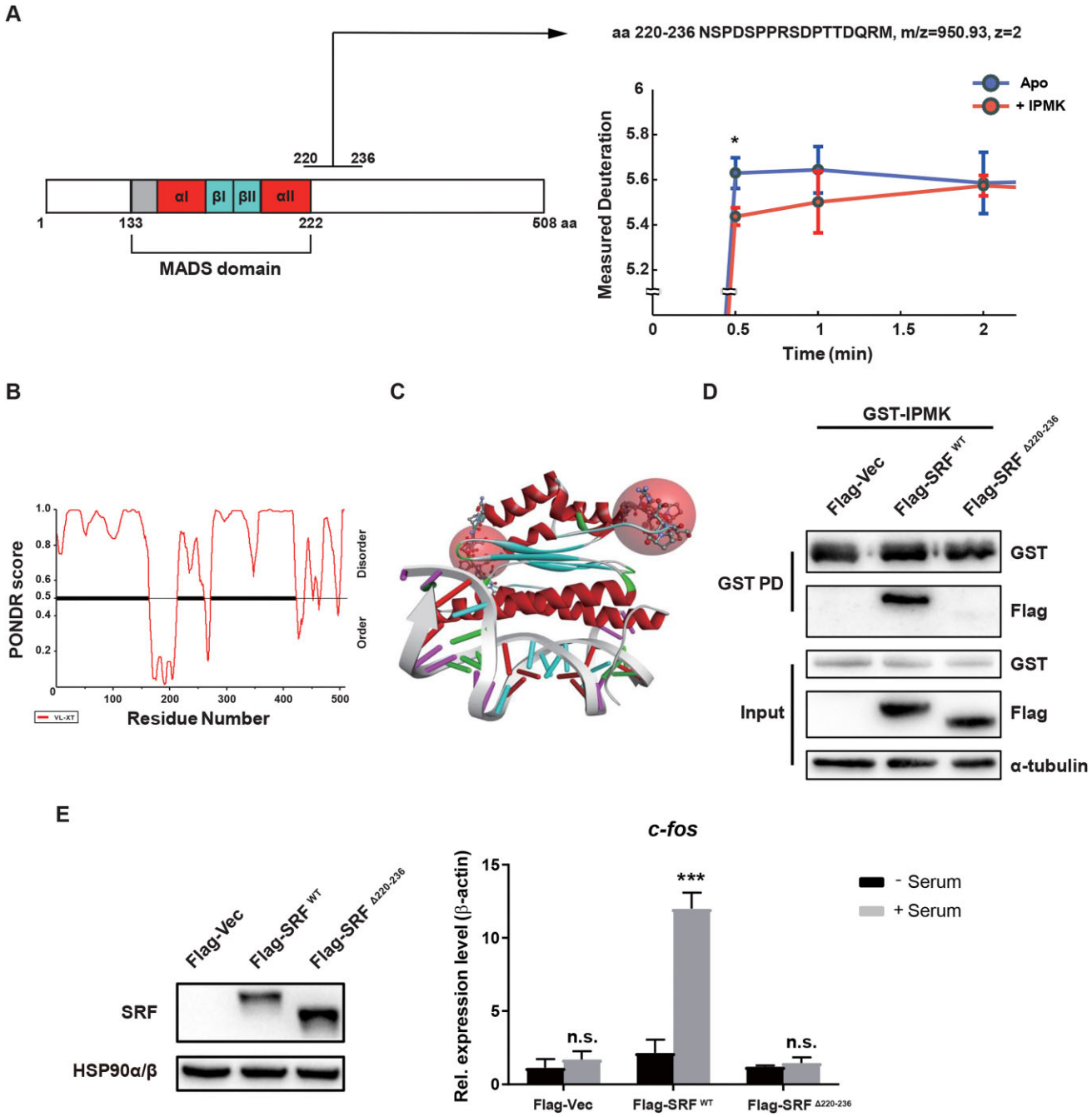

Figure 4. SRF IDR 220–236 interacts with IPMK. (**A**) Domain structure of SRF (left) and a deuterium exchange plot of SRF$^{\Delta 220-236}$ peptide (right). Error bars reflect standard deviations, calculated as Student's *t*-test (*P-value < 0.05). (**B**) Disorder prediction of human SRF using PONDR-VL3 algorithm. The disorder score and the lengths of the predicted disordered regions are indicated. (**C**) Superimpose of DNA-binding SRF crystal (PDB code: 1SRS) and a homology model of SRF (Alphafold UniProt: P11831). Predicted IPMK-SRF binding region was represented as loop structure or ball and stick mode (red sphere). (**D**) Validation of SRF-IPMK binding using GSP pull-down assay. GST-IPMK and Flag-SRF were transfected in HEK293T cells. (**E**) SRF KO NIH3T3 fibroblasts were transfected with Flag-empty, Flag-SRF^{WT} or Flag-SRF SRF$^{\Delta 220-236}$. The messenger RNA levels of the SRF target gene *c-fos* were measured via qPCR. Cells were deprived of serum for 12 h and stimulated with 10% FBS for 30 min. Error bars reflect standard deviations, calculated as Student's *t*-test. Mean ± SEM. ***$P < 0.01$; n.s., not significant.

cific binding between SRF and IPMK. We further investigated whether the interaction between IPMK and SRF is crucial for SRF activity in cells. We generated SRF KO NIH3T3 fibroblasts using CRISPR/Cas9 technology and confirmed that serum responsive *c-fos* induction was significantly impaired in SRF KO cells (Supplementary Figure S8). By transiently overexpressing either wild-type SRF or IPMK-binding defective, mutant SRF (SRF$^{\Delta 220-236}$) in SRF KO fibroblasts, we analyzed *c-fos* expression following serum treatment. Expression of wild-type SRF in SRF KO cells significantly elevated *c-fos* levels in response to serum treatment, whereas SRF$^{\Delta 220-236}$ overexpression failed to rescue SRF KO phenotypes (Figure 4E). These *in vivo* findings clearly suggest that SRF's role in transcription depends on its interaction with IPMK.

When we further characterized the DNA binding of the SRF$^{\Delta 220-236}$ mutant in the presence of IPMK by performing

EMSA, this SRF$^{\Delta 220–236}$ mutant failed to increase SRE binding in the presence of IPMK (Figure 5A and B), validating the key role of SRF IDR 220–236 in mediating IPMK-dependent SRF control. Therefore, our HDX-MS analyses and biochemical studies suggest that the IDR of SRF (220–236) mediates direct binding to IPMK, thereby enhancing SRF–DNA binding. In further single-molecule experiments, we measured the binding fraction using an SRF deletion mutant (SRF$^{\Delta 220–236}$) via sm-FRET. Unlike the results observed with the wild-type SRF (Figure 1B–D), no enhancement in binding of SRF to SRE induced by IPMK was detected using SRF$^{\Delta 220–236}$ (Figure 5C–E). Additionally, the kinetics of the mutant were quantified using smPIFE, which revealed no significant changes in the on-off rates or K_d values in response to IPMK added (Figure 5F–H, Supplementary Figure S9 and Supplementary Table S4). These findings reaffirm that the region of amino acids 220–236 is a critical determinant in modulating the IPMK-dependent DNA-binding activity of SRF.

IPMK induces structural changes in SRF

To investigate whether the interaction with IPMK triggers a conformational change in the SRFs, we directly examined the structural changes within the SRF using three-color single-molecule imaging (Figure 6A). The SRF was site-specifically double-labeled at C218 with Cy5 via thiol-maleimide chemistry and at the N-terminus with Cy3 via ybbR-tag chemistry (42), to monitor a conformational change in SRF. In contrast, the SRE was labeled with Alexa488 at the 5′ end and IPMK was not labeled (Figure 6A). In this experiment, Alexa488 was first visualized for 5 s (cyan color in Figure 6B) and images in which fluorescent signals were detected for all three fluorophores (Alexa488, Cy3 and Cy5) were first selected to analyze the smFRET signals emitted by the SRE–SRF complexes. A representative single-molecule time-trajectory in the absence of IPMK showed a high FRET value of ∼0.7 (top panel in Figure 6B), whereas a low FRET value of ∼0.2 became dominant in the presence of IPMK (middle and bottom panel in Figure 6B). The major peak of the histogram obtained from all the smFRET trajectories shifted from ∼0.7 in the absence of IPMK (top panel in Figure 6C) to ∼0.2 in the presence of 100 nM and 200 nM IPMK (middle and bottom in Figure 6C). As the concentration of IPMK increased, the fraction of low FRET increased (Figure 6D). Such FRET changes suggest that the interaction with IPMK triggers intramolecular structural changes in SRFs and facilitates the binding of SRF to SRE, as shown in Figure 1C. The further analysis revealed the dwell time of SRF in the low FRET ($E_{FRET} < 0.5$) state increased, whereas that in high FRET ($E_{FRET} > 0.5$) state stayed the same as a function of IPMK concentration. Moreover, the dwell time of SRF in the low FRET state is longer than that in the high FRET state (Figure 6E). This data indicates that the low and high FRET states correspond to the stable and transient binding events as in Figure 2.

To delve deeper, we employed a new method to immobilize SRF proteins on a surface, as described in the 'Materials and methods' section. In the presence of IPMK, the dominant FRET values of dual-labeled SRF changed significantly from ∼0.8 to 0.2 (Figure 7A, C, D and E). Conversely, the presence or absence of SRE did not induce such changes (Figure 7A and B). These results indicate that the conformational changes were induced by IPMK rather than SRE. Similarly, when experiments were conducted with the mutant variant (i.e. SRF$^{\Delta 220–236}$), neither the presence nor absence of SRE nor IPMK resulted in structural changes (Supplementary Figure S10).

Discussion

SRF is the founding member of the MADS-box family of transcription factors and is among the most thoroughly characterized DNA-binding proteins in the human proteome (2,12). Despite the universal requirement for SRF to bind a highly specific recognition element in its target gene promoters to induce transcription, the DNA-binding and stabilization process is still surprisingly poorly understood. To fill this knowledge gap, we investigated the molecular mechanisms through which IPMK as a transcriptional coactivator determines the function of SRF. Our multidimensional analyses provide several lines of evidence to show that IPMK induced conformational changes of SRF and enhances SRF–DNA interaction by directly binding to SRF. (i) Both EMSA and single-molecule FRET analyses showed that IPMK enhanced the DNA binding of SRF in a dose-dependent manner. (ii) Single-molecule PIFE studies revealed that the binding of SRF to SRE was significantly increased by IPMK. (iii) Real-time tracking of SRF loci in live cell nuclei showed that the residence time of SRF on the chromatin was decreased by the depletion of IPMK. Conversely, IPMK overexpression stimulates the SRF–chromatin association in cells. (iv) HDX-MS, biochemical and cell biological analyses determined that IPMK binds to the IDR region of SRF adjacent to its DNA binding and dimerization domains. (v) Finally, single-molecule FRET studies indicated that IPMK can induce conformational changes of SRF.

How does the IPMK/SRF association enhance SRF–DNA interaction? Here we proposed a mechanism based on our finding that IPMK enhances the binding of SRF to SRE, the fact that the EMSA pattern of the complexes contained both SRE and SRF but not IPMK, and the structural information of the SRE–SRF complex (50). The equilibrium between temporary and stable SRF-SRE complexes shifts from temporary to stable binding in the presence of IPMK. This shift is governed by conformational changes of SRF via transient interaction with IPMK in a concentration-dependent manner without the formation of stable triple complexes between SRE, SRF and IPMK. The conformational changes induced by IPMK are reminiscent of the chaperone-like activity of Hsp33. Hsp33 is a chaperone that regulates protein conformation without using ATP, relying on its IDR in response to oxidative stress (51–54). Due to this similarity, we refer to the novel function of IPMK as chaperone-like activity. We attribute the chaperone-like activity to the function of certain molecules or proteins that assist other proteins in achieving or maintaining their proper folded structure for protein activation. Unlike true chaperones, chaperone-like molecules may not require ATP and can stabilize the structure of partially folded or IDR structures via protein-protein interactions, promoting correct folding pathways or refolding without forming stable complexes with the target proteins (53,54). Among the two parameters (τ_{on1} and τ_{on2}) determined during the process of SRE–SRF complex formation (Figure 2C and D), τ_{on1}, corresponding to the bound time of weaker and transient binding, may arise from the intrinsic binding between SRE and SRF without IPMK, whereas τ_{on2}, corresponding to the bound time

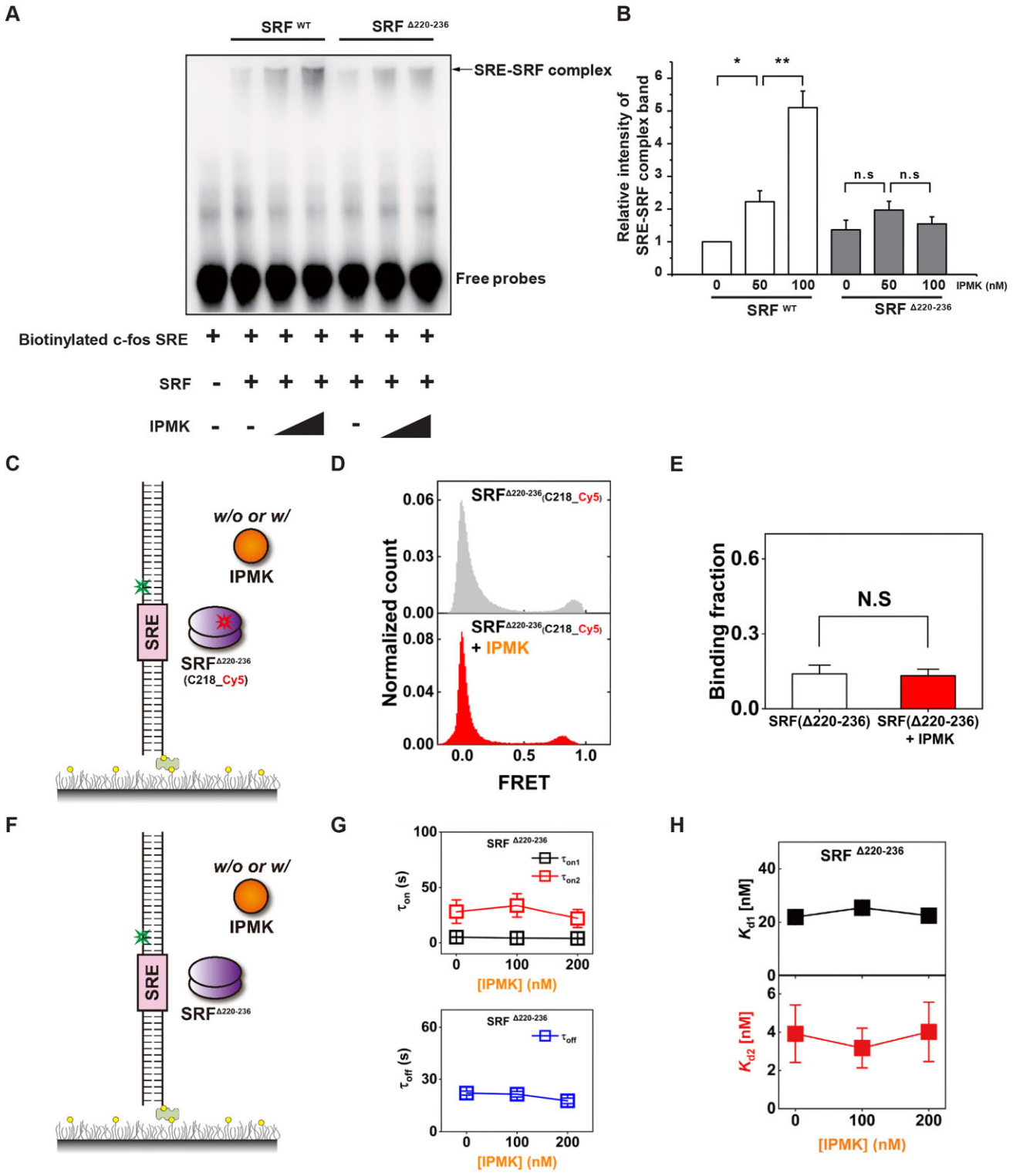

Figure 5. In the presence of IPMK, enhanced binding to the SRE is not observed in the SRF deletion mutant ($SRF^{\Delta 220–236}$). (**A**) EMSA using 1 nM of 5′ biotinylated *c-fos* DNA probe and recombinant His-SRF^{WT}, His-$SRF^{\Delta 220–236}$ (25 nM) and IPMK (50, 100 nM). (**B**) Quantification of the EMSA results (mean values ± SEM of four independent experiments). Error bars reflect standard deviations, calculated as Student's *t*-test, **P*-value < 0.05; ***P*-value < 0.01; n.s., not significant). (**C**) Schematic of single-molecule binding assay of Cy5-$SRF^{\Delta 220–236}$ to Cy3-SRE. (**D**) smFRET histogram of binding of Cy5-$SRF^{\Delta 220–236}$ at 15 nM to SRE after 10-min incubation in the absence (top) or presence (bottom) of IPMK at 100 nM. (**E**) Binding fraction of (**D**) with mean ± SEM (n > 3). Student *t*-test calculated that the difference was not significant (N.S). (**F**) Schematic of single-molecule PIFE assay using Cy3-SRE with $SRF^{\Delta 220–236}$. (**G**) τ_{on1} (black) and τ_{on2} (red) of $SRF^{\Delta 220–236}$ as a function of IPMK concentration (top). And, τ_{off} (blue) (bottom). (**H**) IPMK-concentration-dependence of K_{d1} (top) and K_{d2} (bottom) of $SRF^{\Delta 220–236}$, obtained from (**G**).

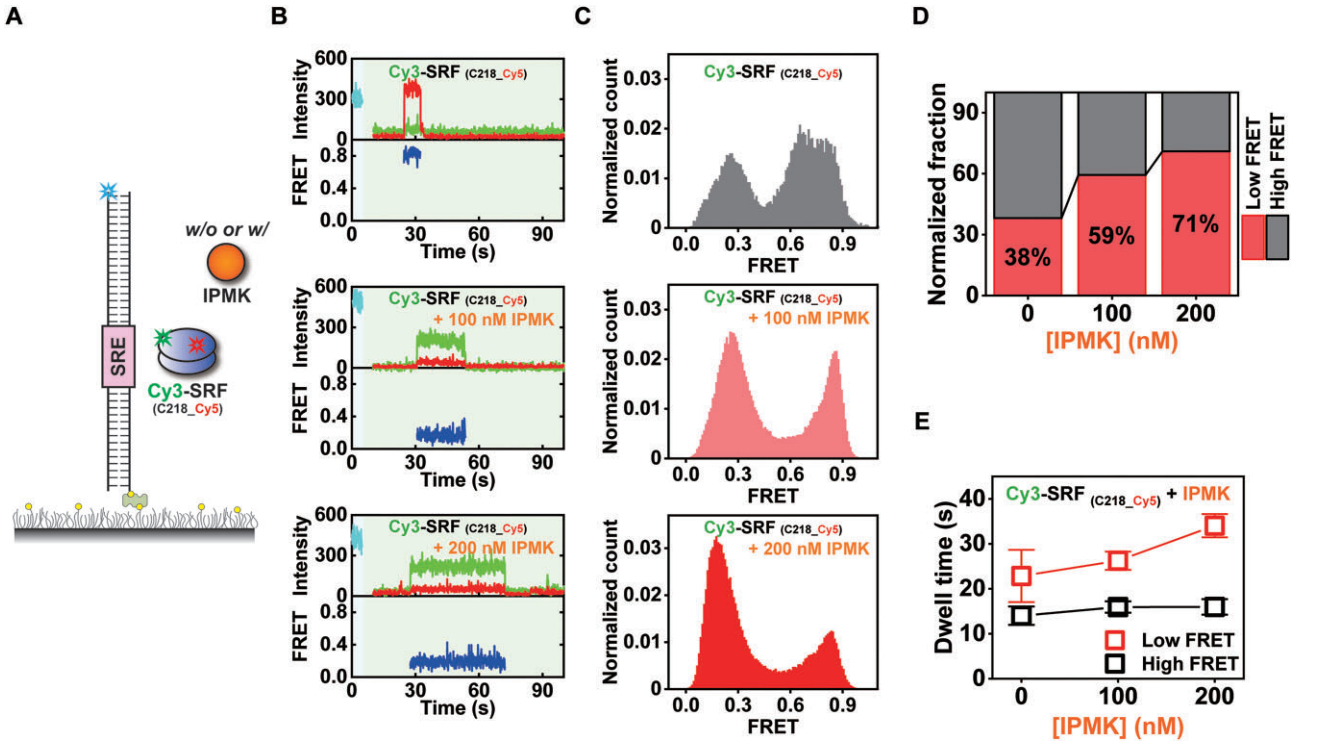

Figure 6. The enhanced binding activity of SRF to SRE results from conformational changes in SRF induced by the interaction with IPMK. (**A**) Schematic of smFRET assay to detect conformational changes of SRF using SRF labeled with Cy3 at the N-terminal and Cy5 at the C218, when SRF binds to SRE in the absence or presence of IPMK. (**B**) Representative fluorescence intensity and FRET time trajectories in the absence (top), presence of 100 nM IPMK (middle) and 200 nM IPMK (bottom). Only the SRE-bound SRF complexes were analyzed by co-localization of Alexa488 (SRE), Cy3 (N-terminal of SRF) and Cy5 (C218 of SRF). (**C**) Corresponding FRET histograms obtained from double-labeled SRFs bound to SREs to SREs in the absence (top), presence of 100 nM IPMK (middle) and presence of 200 nM IPMK (bottom). (**D**) Plot of normalized low FRET fraction ($E_{FRET} < 0.5$) as a function of the IPMK concentration based on data from (**C**). (**E**) Analysis of dwell times in the FRET time trajectory for Cy3-SRF in the absence and presence of IPMK (100 and 200 nM), segmented into low FRET ($E_{FRET} < 0.5$) and high FRET ($E_{FRET} > 0.5$) states. The total analyzed events were 186 for double-labeled SRF alone, 672 for double-labeled SRF with 100 nM IPMK, and 675 for double-labeled SRF with 200 nM IPMK. Data are presented as mean ± SEM.

of stable binding, may arise from and increases with increasing IPMK concentration. This conjecture is further supported by the fact that τ_{on2} is affected by the IPMK concentration but not by τ_{on1} (Figure 2D).

The SRF–DNA interaction enhanced by the non-catalytic function of IPMK uncovered in this study suggests the importance of IDR–IDR interactions between SRF and IPMK. IDRs are being increasingly recognized as mediators of many essential biological functions (55,56). Importantly, IDRs found in TFs appeared to regulate protein stability and functions by providing targets for proteolysis or to mediate macromolecular interactions (e.g. protein–protein, protein–DNA and protein–RNA interactions) (49). Thus, IDRs in TFs can regulate and accelerate the TF search for target promoters by recognizing broad DNA regions (57,58). According to our findings (Figure 4), the IDR of SRF, which is located near its dimerization region and other cofactor binding regions, appears to provide a key interface for IPMK binding, thus enabling stable SRF–DNA interactions. The decreased residence time of SRF for chromatin binding under IPMK depletion was indeed demonstrated by tracking Halo-SRF dynamics in live cells at the single-molecule level.

The increase of τ_{on2} could indicate an inherent heterogeneity in SRF's interaction with DNA, potentially due to SRF's structural flexibility (i.e. IDR) or its ability to adopt multiple binding conformations naturally. The SRF may exhibit a rugged energy landscape due to the IDR, meaning it has multiple low-energy states that the protein can adopt. This characteristic allows the IDR to explore a variety of conformations, enabling flexibility in its structure. When interacting with DNA, this flexibility permits the IDR to sample different conformational states, optimizing its binding to the DNA and facilitating protein–DNA interactions with various regions of the target molecule. This adaptability is crucial for dynamic protein–DNA interactions, as it allows the IDR to shift between conformations that stabilize binding, modulate interaction strength through the interaction with IPMK in a concentration-dependent manner. This implies that the flexible structure of SRF is suitable to multiple DNA-binding configurations. This is evidenced by the very wide distribution of Figure 6C, although current single-molecule technologies have spatiotemporal limitations in their ability to distinguish different degrees of fine conformations.

The non-catalytic activities of kinase proteins have drawn increasing attention, as they add another layer of complexity to gene expression control (59). For example, p38alpha/beta MAP kinase directly binds to the transcriptional activator Mirk/Dyrk1B, thereby blocking its activity (60). EGFR lacks a DNA binding domain but can interact with several transcription factors such as STATs3/5 and E2F1 to activate the expression of genes such as iNOS and COX-2 (61). A C-terminal ERBB4 kinase fragment lacking the catalytic domain is able to activate transcription by associating with TFs (e.g.

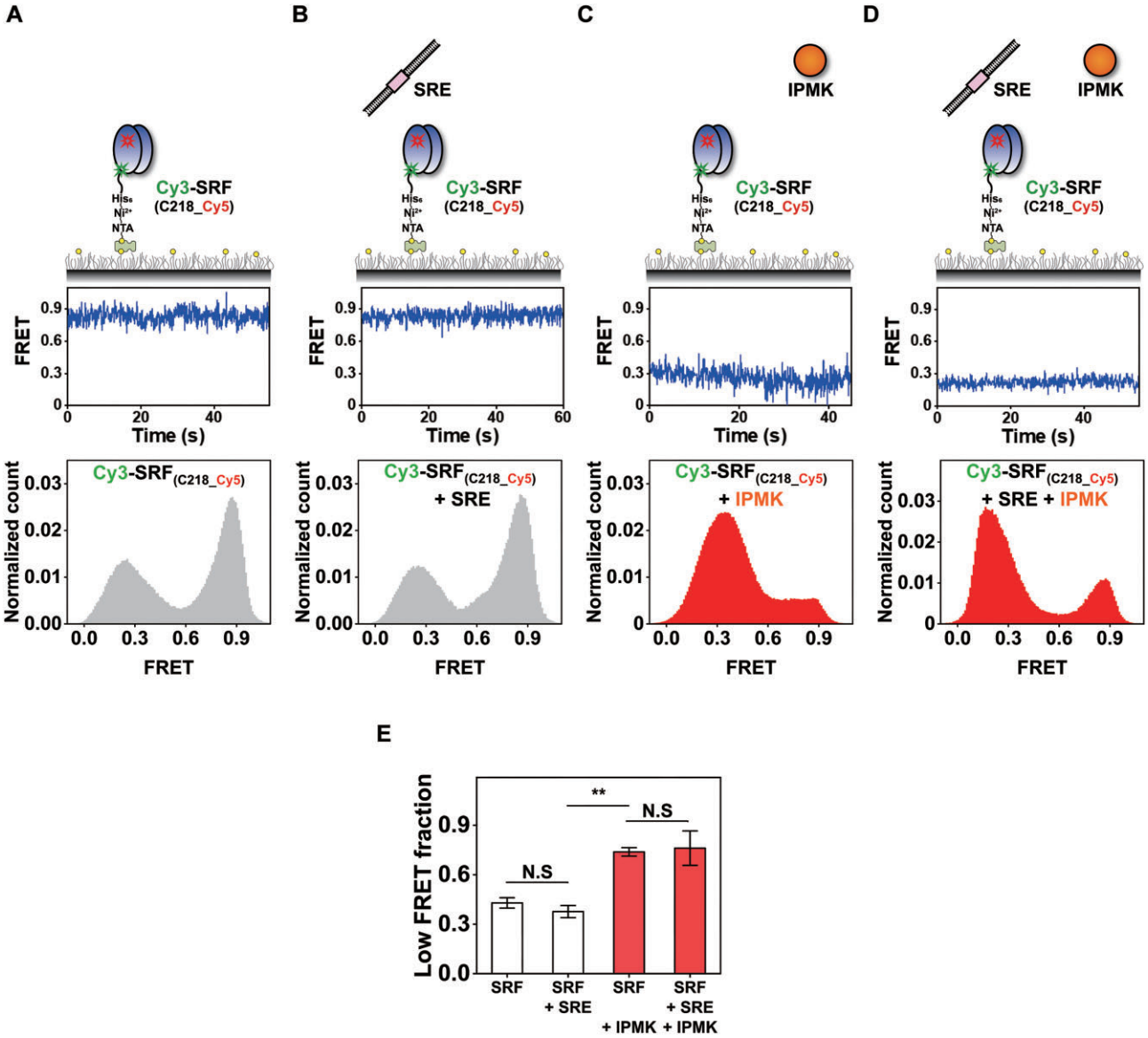

Figure 7. IPMK-induced conformational change of SRF, independent of SRE. (**A–D**) Schematic illustrations of smFRET assay by using immobilization double labeled SRFs (top). SRF alone (**A**), with SRE (**B**), with IPMK (**C**), and with both SRE and IPMK (**D**). Representative FRET trajectories corresponding to each condition (middle). Corresponding FRET histograms obtained from double-labeled SRFs (bottom). The number of traces analyzed in the panels (**A**)–(**D**) were 341, 262, 1320 and 425, respectively. (**E**) Quantitative analysis of the low FRET fraction from the histograms. Error bars denote the mean ± SEM (n = 3), with $^{**}P$ value < 0.01.

YAP, STAT5A) in the nucleus (62,63). The mechanism through which IPMK restrains SRF in a functionally competent conformation seems unique, as there are no previous examples of the stabilization of DNA–TF interactions by a kinase enzyme. This highlights the complexity of the non-catalytic roles of kinases in transcription control. Similar versatility can be found in APE1 (also known as Ref-1), which acts as an AP endonuclease in the base excision repair (BER) pathway but also enhances the binding activity of several cancer-associated TFs (64).

Taken together, our findings suggest that IDR-mediated interaction between IPMK and SRF is a pivotal mechanism for SRF-dependent gene expression. This is achieved by inducing conformational changes on SRF at specific genomic sites (i.e. increasing the τ_{on2}). Given that SRF is essential for organogenesis and has been linked to a number of diseases such as cancer, our results suggest that the modulation of IPMK levels and SRF-binding activities contribute to the regulation of transcriptional efficiency, as well as disease progression. An imbalance in the levels of IPMK and SRF proteins in the human body has been implicated in a number of developmental diseases as well as cancer. Therefore, additional studies are needed to gain further insights into the regulatory mechanism underlying IPMK-SRF binding, as this would provide a basis for the development of novel therapeutic strategies to control SRF-driven pathologies such as cancer cell proliferation and metastasis.

Data availability

All data are available from the corresponding authors upon reasonable request.

Supplementary data

Supplementary Data are available at NAR Online.

Acknowledgements

Author contributions: W.C., G.L. and S.K. conceived the work. H.A., J.Y., J.R., S.K., J.Y.P., J.K.K., I.J., H.A., S.H., S.M., M.A., K.R., E.K., K.P., M.A. and T.L. performed the experiments. Y.B., J.S., J.K., I.J. and D.L. provided reagents and technical comments. H.A., J.Y., K.R., W.C., G.L. and S.K. designed the experiments, analyzed the data and wrote the manuscript. We thank the members of the Cho, Lee and Kim laboratory for their assistance and advice.

Funding

National Research Foundation of Korea [NRF-2020R1C1C1014599 to W.C.; NRF-2022R1A4A2000790, RS-2024-00408712 and RS-2024-00341654 to G.L.; and NRF-2018R1A5A1024261, RS-2023-00278918 and RS-2024-00415888 to S.K.]; Samsung Foundation of Science & Technology [SSTF-BA1401-14 to S.K.]; Suh Kyungbae Foundation (to W.C.).

Conflict of interest statement

None declared.

References

1. Treisman,R. and Ammerer,G. (1992) The SRF and MCM1 transcription factors. *Curr. Opin. Genet. Dev.*, **2**, 221–226.
2. Norman,C., Runswick,M., Pollock,R. and Treisman,R. (1988) Isolation and properties of cDNA clones encoding SRF, a transcription factor that binds to the c-fos serum response element. *Cell*, **55**, 989–1003.
3. Wang,D.Z. and Olson,E.N. (2004) Control of smooth muscle development by the myocardin family of transcriptional coactivators. *Curr. Opin. Genet. Dev.*, **14**, 558–566.
4. Niu,Z., Yu,W., Zhang,S.X., Barron,M., Belaguli,N.S., Schneider,M.D., Parmacek,M., Nordheim,A. and Schwartz,R.J. (2005) Conditional mutagenesis of the murine serum response factor gene blocks cardiogenesis and the transcription of downstream gene targets. *J. Biol. Chem.*, **280**, 32531–32538.
5. Miano,J.M., Ramanan,N., Georger,M.A., De Mesy Bentley,K.L., Emerson,R.L., Balza,R.O., Xiao,Q., Weiler,H., Ginty,D.D. and Misra,R.P. (2004) Restricted inactivation of serum response factor to the cardiovascular system. *Proc. Natl Acad. Sci. U.S.A.*, **101**, 17132–17137.
6. Parlakian,A., Charvet,C., Escoubet,B., Mericskay,M., Molkentin,J.D., Gary-Bobo,G., De Windt,L.J., Ludosky,M.A., Paulin,D., Daegelen,D., *et al.* (2005) Temporally controlled onset of dilated cardiomyopathy through disruption of the srf gene in adult heart. *Circulation*, **112**, 2930–2939.
7. Knöll,B., Kretz,O., Fiedler,C., Alberti,S., Schütz,G., Frotscher,M. and Nordheim,A. (2006) Serum response factor controls neuronal circuit assembly in the hippocampus. *Nat. Neurosci.*, **9**, 195–204.
8. Arsenian,S., Weinhold,B., Oelgeschläger,M., Rüther,U. and Nordheim,A. (1998) Serum response factor is essential for mesoderm formation during mouse embryogenesis. *EMBO J.*, **17**, 6289–6299.
9. Miano,J.M. (2010) Role of serum response factor in the pathogenesis of disease. *Lab. Investig.*, **90**, 1274–1284.
10. Deshpande,A., Shetty,P.M.V., Frey,N. and Rangrez,A.Y. (2022) SRF: a seriously responsible factor in cardiac development and disease. *J. Biomed. Sci.*, **29**, 1–21.
11. Azam,H., Pierro,L., Reina,M., Gallagher,W.M. and Prencipe,M. (2022) Emerging role for the serum response factor (SRF) as a potential therapeutic target in cancer. *Expert Opin. Ther. Targets*, **26**, 155–169.
12. Miano,J.M. (2003) Serum response factor: toggling between disparate programs of gene expression. *J. Mol. Cell. Cardiol.*, **35**, 577–593.
13. Onuh,J.O. and Qiu,H. (2020) The serum response factor/cofactors interactions and their implications in diseases. *FEBS J.*, **288**, 3120–3134.
14. Dalton,S., Marais,R., Wynne,J. and Treisman,R. (1993) Isolation and characterization of SRF accessory proteins. *Philos. Trans. R. Soc. Lond. B. Biol. Sci.*, **340**, 325–332.
15. Posern,G. and Treisman,R. (2006) Actin' together: serum response factor, its cofactors and the link to signal transduction. *Trends Cell Biol.*, **16**, 588–596.
16. Olson,E.N. and Nordheim,A. (2010) Linking actin dynamics and gene transcription to drive cellular motile functions. *Nat. Rev. Mol. Cell Biol.*, **11**, 353–365.
17. Gualdrini,F., Esnault,C., Horswell,S., Stewart,A., Matthews,N. and Treisman,R. (2016) SRF co-factors control the balance between cell proliferation and contractility. *Mol. Cell*, **64**, 1048–1061.
18. Wang,Z., Wang,D., Hockemeyer,D., Mcanally,J., Nordheim,A. and Olson,E.N. (2004) Myocardin and ternary complex factors compete for SRF to control smooth muscle gene expression. **428**, 185–189.
19. Kim,E., Tyagi,R., Lee,J.Y., Park,J., Kim,Y.R., Beon,J., Chen,P.Y., Cha,J.Y., Snyder,S.H. and Kim,S. (2013) Inositol polyphosphate multikinase is a coactivator for serum response factor-dependent induction of immediate early genes. *Proc. Natl Acad. Sci. U.S.A.*, **110**, 19938–19943.
20. Saiardi,A., Erdjument-Bromage,H., Snowman,A.M., Tempst,P. and Snyder,S.H. (1999) Synthesis of diphosphoinositol pentakisphosphate by a newly identified family of higher inositol polyphosphate kinases. *Curr. Biol.*, **9**, 1323–1326.
21. Maag,D., Maxwell,M.J., Hardesty,D., Boucher,K.L., Choudhari,N., Hanno,A.G., Ma,J.F., Snowman,A.S., Pietropaoli,J.W., Xu,R., *et al.* (2011) Inositol polyphosphate multikinase is a physiologic PI3-kinase that activates Akt/PKB. *Proc. Natl Acad. Sci. U.S.A.*, **108**, 1391–1396.
22. Kim,S., Bhandari,R., Brearley,C.A. and Saiardi,A. (2024) The inositol phosphate signalling network in physiology and disease. *Trends. Biochem. Sci.*, **49**, 969–985.
23. Nagpal,L., He,S., Rao,F. and Snyder,S.H. (2024) Inositol pyrophosphates as versatile metabolic messengers. *Annu. Rev. Biochem.*, **93**, 317–338.
24. Kim,S., Kim,S.F., Maag,D., Maxwell,M.J., Resnick,A.C., Juluri,K.R., Chakraborty,A., Koldobskiy,M.A., Cha,S.H., Barrow,R., *et al.* (2011) Amino acid signaling to mTOR mediated by inositol polyphosphate multikinase. *Cell Metab.*, **13**, 215–221.
25. Kim,E., Beon,J., Lee,S., Park,S.J., Ahn,H., Kim,M.G., Park,J.E., Kim,W., Yuk,J.-M., Kang,S.-J., *et al.* (2017) Inositol polyphosphate multikinase promotes toll-like receptor–induced inflammation by stabilizing TRAF6. *Sci. Adv.*, **3**, e1602296.
26. Beon,J., Han,S., Yang,H., Park,S.E., Hyun,K., Lee,S.-Y., Rhee,H.-W., Seo,J.K., Kim,J., Kim,S., *et al.* (2022) Inositol polyphosphate multikinase physically binds to the SWI/SNF complex and modulates BRG1 occupancy in mouse embryonic stem cells. *eLife*, **11**, e73523.
27. Hong,S., Kim,K., Shim,Y.R., Park,J., Choi,S.E., Min,H., Lee,S., Song,J.J., Kang,S.J., Jeong,W.I., *et al.* (2024) A non-catalytic role of IPMK is required for PLCγ1 activation in T cell receptor signaling by stabilizing the PLCγ1-Sam68 complex. *Cell Commun. Signal.*, **22**, 526.
28. El Bakkoury,M., Dubois,E. and Messenguy,F. (2000) Recruitment of the yeast MADS-box proteins, ArgRI and Mcm1 by the pleiotropic factor ArgRIII is required for their stability. *Mol. Microbiol.*, **35**, 15–31.

29. Odom,A.R., Stahlberg,A., Wente,S.R. and York,J.D. (2000) A role for nuclear inositol 1,4,5-trisphosphate kinase in transcriptional control. *Science*, **287**, 2026–2029.
30. Blind,R.D., Suzawa,M. and Ingraham,H.A. (2012) Direct modification and activation of a nuclear receptor-PIP2 complex by the inositol lipid kinase IPMK. *Sci. Signal.*, **5**, ra44–ra44.
31. Hwang,H. and Myong,S. (2014) Protein induced fluorescence enhancement (PIFE) for probing protein–nucleic acid interactions. *Chem. Soc. Rev.*, **43**, 1221–1229.
32. Tinevez,J.Y., Perry,N., Schindelin,J., Hoopes,G.M., Reynolds,G.D., Laplantine,E., Bednarek,S.Y., Shorte,S.L. and Eliceiri,K.W. (2017) TrackMate: an open and extensible platform for single-particle tracking. *Methods*, **115**, 80–90.
33. Loffreda,A., Jacchetti,E., Antunes,S., Rainone,P., Daniele,T., Morisaki,T., Bianchi,M.E., Tacchetti,C. and Mazza,D. (2017) Live-cell p53 single-molecule binding is modulated by C-terminal acetylation and correlates with transcriptional activity. *Nat. Commun.*, **8**. 313.
34. Labun,K., Montague,T.G., Krause,M., Cleuren,Y.N.T., Tjeldnes,H. and Valen,E. (2019) CHOPCHOP v3: expanding the CRISPR web toolbox beyond genome editing. *Nucleic Acids Res.*, **47**, W171–W174.
35. Shalem,O., Sanjana,N.E., Hartenian,E., Shi,X., Scott,D.A., Mikkelson,T., Heckl,D., Ebert,B.L., Root,D.E., Doench,J.G., *et al.* (2014) Genome-scale CRISPR-Cas9 knockout screening in human cells. *Science*, **343**, 84–87.
36. Cox,J. and Mann,M. (2008) MaxQuant enables high peptide identification rates, individualized p.p.b.-range mass accuracies and proteome-wide protein quantification. *Nat. Biotechnol.*, **26**, 1367–1372.
37. Cox,J., Neuhauser,N., Michalski,A., Scheltema,R.A., Olsen,J.V. and Mann,M. (2011) Andromeda: a peptide search engine integrated into the MaxQuant environment. *J. Proteome Res.*, **10**, 1794–1805.
38. Raval,S., Sarpe,V., Hepburn,M., Crowder,D.A., Zhang,T., Viner,R. and Schriemer,D.C. (2021) Improving spectral validation rates in hydrogen–deuterium exchange data analysis. *Anal. Chem.*, **93**, 4246–4254.
39. Rey,M., Sarpe,V., Burns,K.M., Buse,J., Baker,C.A.H., van Dijk,M., Wordeman,L., Bonvin,A.M.J.J. and Schriemer,D.C. (2014) Mass spec studio for integrative structural biology. *Structure*, **22**, 1538–1548.
40. Roy,R., Hohng,S. and Ha,T. (2008) A practical guide to single-molecule FRET. *Nat. Methods*, **5**, 507–516.
41. Koh,H.R., Roy,R., Sorokina,M., Tang,G.Q., Nandakumar,D., Patel,S.S. and Ha,T. (2018) Correlating transcription initiation and conformational changes by a single-subunit RNA polymerase with near base-pair resolution. *Mol. Cell*, **70**, 695–706.
42. Yin,J., Straight,P.D., McLoughlin,S.M., Zhou,Z., Lin,A.J., Golan,D.E., Kelleher,N.L., Kolter,R. and Walsh,C.T. (2005) Genetically encoded short peptide tag for versatile protein labeling by Sfp phosphopantetheinyl transferase. *Proc. Natl Acad. Sci. U.S.A.*, **102**, 15815–15820.
43. Akaike,H. (1974) A new look at the statistical model identification. *IEEE Trans. Autom. Control*, **19**, 716–723.
44. Schwarz,G. (1078) Estimating the dimension of a model. *Ann. Statist.*, **6**, 461–464.
45. Shyu,Y.J., Suarez,C.D. and Hu,C.-D. (2008) Visualization of AP-1–NF-kappaB ternary complexes in living cells by using a BiFC-based FRET. *Proc. Natl. Acad. Sci. U.S.A*, **105**, 151–156.
46. Zappavigna,V., Falciola,L., Citterich,M.H., Mavilio,F. and Bianchi,M.E. (1996) HMG1 interacts with HOX proteins and enhances their DNA binding and transcriptional activation. *EMBO J.*, **15**, 4981–4991.
47. Hipp,L., Beer,J., Kuchler,O., Reisser,M., Sinske,D., Michaelis,J., Gebhardt,J.C.M. and Knöll,B. (2019) Single-molecule imaging of the transcription factor SRF reveals prolonged chromatin-binding kinetics upon cell stimulation. *Proc. Natl Acad. Sci. U.S.A.*, **116**, 880–889.
48. Seacrist,C.D. and Blind,R.D. (2018) Crystallographic and kinetic analyses of human IPMK reveal disordered domains modulate ATP binding and kinase activity. *Sci. Rep.*, **8**, 1–12.
49. Obradovic,Z. (2005) With protein evolutionary information. *J. Bioinform. Comput. Biol.*, **3**, 35–60.
50. Pellegrini,L., Tan,S. and Richmond,T.J. (1995) Structure of serum response factor core bound to DNA. *Nature*, **376**, 490–498.
51. Jakob,U., Muse,W., Eser,M. and Bardwell,J.C. (1999) Chaperone activity with a redox switch. *Cell*, **96**, 341–352.
52. Reichmann,D., Xu,Y., Cremers,C.M., Ilbert,M., Mittelman,R., Fitzgerald,M.C. and Jakob,U. (2012) Order out of disorder: working cycle of an intrinsically unfolded chaperone. *Cell*, **148**, 947–957.
53. Mitra,R., Wu,K., Lee,C. and Bardwell,J.C.A. (2022) ATP-independent chaperones. *Annu. Rev. Biophys.*, **51**, 409–429.
54. Sus,O. and Reichmann,D. (2015) Protein plasticity underlines activation and function of ATP-independent chaperones. *Front Mol. Biosci.*, **2**, 43.
55. Perdigão,N., Heinrich,J., Stolte,C., Sabir,K.S., Buckley,M.J., Tabor,B., Signal,B., Gloss,B.S., Hammang,C.J., Rost,B., *et al.* (2015) Unexpected features of the dark proteome. *Proc. Natl Acad. Sci. U.S.A.*, **112**, 15898–15903.
56. Wright,P.E. and Dyson,H.J. (2015) Intrinsically disordered proteins in cellular signalling and regulation. *Nat. Rev. Mol. Cell Biol.*, **16**, 18–29.
57. Fuxreiter,M., Simon,I. and Bondos,S. (2011) Dynamic protein–DNA recognition: beyond what can be seen. *Trends Biochem. Sci.*, **36**, 415–423.
58. Garcia,D.A., Johnson,T.A., Presman,D.M., Fettweis,G., Wagh,K., Rinaldi,L., Stavreva,D.A., Paakinaho,V., Jensen,R.A.M., Mandrup,S., *et al.* (2021) An intrinsically disordered region-mediated confinement state contributes to the dynamics and function of transcription factors. *Mol. Cell*, **81**, 1484–1498.
59. Rauch,J., Volinsky,N., Romano,D. and Kolch,W. (2011) The secret life of kinases: functions beyond catalysis. *Cell Commun. Signal.*, **9**, 1–28.
60. Lim,S., Zou,Y. and Friedman,E. (2002) The transcriptional activator Mirk/Dyrk1B is sequestered by p38α/β MAP kinase. *J. Biol. Chem.*, **277**, 49438–49445.
61. Wang,Y.N., Yamaguchi,H., Hsu,J.M. and Hung,M.C. (2010) Nuclear trafficking of the epidermal growth factor receptor family membrane proteins. *Oncogene*, **29**, 3997–4006.
62. Aqeilan,R.I., Donati,V., Palamarchuk,A., Trapasso,F., Kaou,M., Pekarsky,Y., Sudol,M. and Croce,C.M. (2005) WW domain-containing proteins, WWOX and YAP, compete for interaction with ErbB-4 and modulate its transcriptional function. *Cancer Res.*, **65**, 6764–6772.
63. Williams,C.C., Allison,J.G., Vidal,G.A., Burow,M.E., Beckman,B.S., Marrero,L. and Jones,F.E. (2004) The ERBB4/HER4 receptor tyrosine kinase regulates gene expression by functioning as a STAT5A nuclear chaperone. *J. Cell Biol.*, **167**, 469–478.
64. Evans,A.R., Limp-Foster,M. and Kelley,M.R. (2000) Going APE over ref-1. *Mutat. Res.*, **461**, 83–108.

Received: September 13, 2024. **Revised:** December 9, 2024. **Editorial Decision:** December 11, 2024. **Accepted:** December 13, 2024